Petroleum Science 21 (2024) 1671–1682

Contents lists available at ScienceDirect

Petroleum Science

journal homepage: www.keaipublishing.com/en/journals/petroleum-science

Original Paper

A reweighted damped singular spectrum analysis method for robust seismic noise suppression

Wei-Lin Huang [a, *], Yan-Xin Zhou [b], Yang Zhou [c], Wei-Jie Liu [a], Ji-Dong Li [a]

[a] State Key Laboratory of Petroleum Resources and Engineering, China University of Petroleum (Beijing), Beijing, 102249, China
[b] SINOPEC Petroleum Exploration and Production Research Institute, Beijing, 102206, China
[c] SINOPEC Geophysical Research Institute, Nanjing, 211103, Jiangsu, China

ARTICLE INFO

Article history:
Received 2 August 2022
Received in revised form
11 January 2024
Accepted 21 January 2024
Available online 11 February 2024

Edited by Jie Hao and Meng-Jiao Zhou

Keywords:
Singular spectrum analysis
Damping operator
Seismic erratic noise
Seismic signal processing
Robust low-rank reconstruction

ABSTRACT

(Multichannel) Singular spectrum analysis is considered as one of the most effective methods for seismic incoherent noise suppression. It utilizes the low-rank feature of seismic signal and regards the noise suppression as a low-rank reconstruction problem. However, in some cases the seismic geophones receive some erratic disturbances and the amplitudes are dramatically larger than other receivers. The presence of this kind of noise, called erratic noise, makes singular spectrum analysis (SSA) reconstruction unstable and has undesirable effects on the final results. We robustify the low-rank reconstruction of seismic data by a reweighted damped SSA (RD-SSA) method. It incorporates the damped SSA, an improved version of SSA, into a reweighted framework. The damping operator is used to weaken the artificial disturbance introduced by the low-rank projection of both erratic and random noise. The central idea of the RD-SSA method is to iteratively approximate the observed data with the quadratic norm for the first iteration and the Tukeys bisquare norm for the rest iterations. The RD-SSA method can suppress seismic incoherent noise and keep the reconstruction process robust to the erratic disturbance. The feasibility of RD-SSA is validated via both synthetic and field data examples.

1. Introduction

Field seismic data are always masked by various incoherent noise. The incoherent noise will degrade quality of sampled data, and negatively affect the final imaging or inversion performance (Wang et al., 2022; Li and Qu, 2022). Therefore, incoherent noise suppression is an indispensable step in seismic data processing.

In the past decades, a lot of effort has been put to denoise seismic data, and a large number of efficient denoising techniques have been proposed. For instance, data decomposition techniques denoise seismic data by first decomposing the noisy seismic data into different components and then reconstructing the signal according to certain attribute. Successful examples include the empirical mode decomposition (Bekara and van der Baan, 2009; Gómez and Velis, 2016) and mathematical morphological decomposition (Wang et al., 2008; Li et al., 2016). Huang et al. (2017a) introduced an orthogonalization operator into traditional decomposition-and-reconstruction framework to improve performance of unveiling weak signal from extremely noisy data. Sparsity-promoting methods remove seismic noise on the basis of the different sparse features between signal and noise. It generally estimates the signal and removes noise by a thresholding or muting operation in a certain sparse domain. Successful examples include the Radon (Trad et al., 2002), Fourier (Zwartjes and Gisolf, 2007), wavelet (Mousavi et al., 2016; Anvari et al., 2017), and curvelet (Herrmann and Hennenfent, 2008; Chen et al., 2022) transforms.

The low-rank approximation technique explores the low-rank feature of seismic signal, which treats the seismic denoising problem as the data matrix decomposition (Lan et al., 2022). Noise or other unwanted incoherent energies increase the rank of the data matrix, and noise suppression can be achieved by reducing the rank of the data matrix. As one of the rank-reduction-based approaches, singular spectrum analysis (SSA) or its multichannel version (MSSA) is widely demonstrated to be effective in denoising of seismic data (Trickett, 2008; Sacchi, 2009; Oropeza and Sacchi, 2011). The core rank-reduction operator in SSA is implemented by a truncated singular value decomposition (SVD) filter (Anvari et al., 2019; Li et al., 2021), which decomposes the vector space of the Hankel/Toeplitz matrix of the observed data into a signal

* Corresponding author.
E-mail address: cup_hwl@126.com (W.-L. Huang).

https://doi.org/10.1016/j.petsci.2024.01.018

subspace and a noise subspace, and then removes the energies in the noise subspace to achieve noise attenuation. Many modified SSA methods have been proposed from different aspects. Huang et al. (2017b) extended the SSA method into randomization domain and develop an algorithm for simultaneous random and coherent noise attenuation. Oropeza and Sacchi (2011) used randomized SVD as fast approximations to the truncated SVD to speed up traditional SSA filtering. For a similar purpose, Cheng and Sacchi (2015) replaced truncated SVD with the more efficient randomized QR decomposition. Naghizadeh and Sacchi (2013) address the problem of interpolation beyond aliasing in the SSA reconstruction.

Although effective, the traditional truncated SVD is a non-robust rank-reduction operator which performs unsteadily when the seismic data are contaminated by erratic interference. This kind of interference is often caused by swell noise, power line noise, air blast noise, artifacts caused by glitches, recording errors and uncorrected polarity reversals. The erratic noise is not a specific kind of noise. If the energy of the noise is relatively concentrated in certain traces or ranges, with an amplitude significantly larger than the effective signal, and without a definite space-time shape (e.g., apparent velocity), it can be called erratic noise. To solve this problem, Trickett et al. (2012) blended SSA into a reweighting iteration framework to robustify the least-squares estimators and thus obtain robust performance in attenuating erratic noise. Similarly, Chen and Sacchi (2014) combined the SSA filter and iteratively reweighed least-squares method to suppress erratic noise. Cheng et al. (2015) applied robust principal component analysis and the first-order gradient iteration method to suppress seismic erratic noise. Bahia and Sacchi (2019) proposed a bifactored gradient descent-based SSA to simultaneously reconstruct and denoise 3D seismic dataset and also deblend simultaneous-source seismic data (Lin et al., 2021). Wu et al. (2020) used L_p-norm robust principal component analysis to a workflow to attenuate seismic traffic noise. In addition to these, Sternfels et al. (2015) modeled the signal and erratic noise as low-rank and sparse components, respectively, and attenuated erratic noise from incomplete seismic data by a joint low-rank and sparse inversion. Zhu et al. (2019) detected and suppressed high amplitude noise using a convolutional neural network. Huang and Liu (2020) proposed to constrain the morphological scale of the data when solving the interpolation problem, which can improve the robustness to the spatial aliasing and erratic energies.

The reweighting iteration SSA and its various analogues deal with the erratic disturbance by iterating the estimation according to the absolute difference between the original and filtered data. However, the method may fail when the data are corrupted by strong erratic disturbance because the low-rank projection in SSA is forced to introduce significant artificial disturbance to fit the high amplitudes of erratic disturbance under the sense of least-squares. Huang et al. (2016) indicated that the truncated SVD in SSA actually decomposes the data into a noise subspace and a signal-plus-noise subspace, and derived a damped SSA (DSSA) which can theoretically remove the noise from the signal-plus-noise subspace. The DSSA method has been demonstrated to be more effective for seismic low-rank interpolation and denoising. In this work, we further extend the DSSA method to robustify the low-rank reconstruction of seismic data, and propose a reweighted version of DSSA (RD-SSA). In the proposed RD-SSA method, the damping operator is used to weaken the artificial disturbance introduced by the low-rank projection of both erratic and random noise. The damping factor can be adjusted to project both erratic and random noise to an acceptable level and avoid the error accumulated with iterations. The prominent advantage of our proposed RD-SSA method is that it is more robust to the strong erratic disturbance. We have tested the proposed RD-SSA method on both synthetic and field seismic data examples and the results demonstrate its feasibility.

2. Theory

2.1. Problem formulations

As many geophysical problems, the additive noise model and denoising can be formulated as a pair of forward and inversion processes as

$$\mathbf{D} = \mathbf{S} + \mathbf{N}, \tag{1}$$

$$\mathbf{S} = \mathrm{argmin}_{\mathbf{S}'} \|\mathbf{D} - \mathbf{S}'\| + \mathscr{R}(\mathbf{S}'), \tag{2}$$

where $\mathbf{D}$ is the 2D observed data in time domain. $\mathbf{S}$ and $\mathbf{N}$ are the noise-free signal and incoherent noise with the same size, dimension and domain with $\mathbf{D}$. $\mathscr{R}$ denotes the regularization operator and $\|\cdot\|$ stands for the certain norm. $\mathbf{S}'$ represents a temporary variable in the minimization problem. In general, the first term in Eq. (2) is called fidelity term which ensures that the estimated signal $\mathbf{S}$ agrees with the observation, and the second term is the penalty term which forces some prior constraints to the estimated signal $\mathbf{S}$ (Ding and Selesnick, 2015; Chen et al., 2019). The different combinations of fidelity and penalty terms define different denoising methods. In most cases, the incoherent noise $\mathbf{N}$ is assumed to obey a Gaussian distribution, and the norm $\|\cdot\|$ is chosen as the Frobenius norm.

2.2. Reweighted damped SSA

The denoising problem can be solved by the SSA approach, which provides us a filter of ω frequency component $\mathbf{D}^{\omega}$ to denoise seismic data consisting of three main steps as (Oropeza and Sacchi, 2011)

$$\mathbf{S}'^{\omega} = \mathcal{P}\_\{\mathcal{A}\}(\mathcal{P}\_\{\mathcal{R}\}(\mathcal{P}\_\{\mathcal{H}\}(\mathbf{D}^{\omega}))), \tag{3}$$

where $\mathcal{P}\_\{\mathcal{H}\}$ is a rearranging operator to rearrange the data $\mathbf{D}^{\omega}$ into a Hankel structure as

$$\mathbf{H}^{\omega} = \mathcal{P}\_\{\mathcal{H}\}(\mathbf{D}^{\omega}) = \begin{pmatrix} D(1) & D(2) & \cdots & D(y) \\ D(2) & D(3) & \cdots & D(y+1) \\ \vdots & \vdots & \ddots & \vdots \\ D(x) & D(x+1) & \cdots & D(N) \end{pmatrix}, \tag{4}$$

where $D(1), D(2), \ldots, D(N)$ are the elements of $\mathbf{D}^{\omega}$. $x = N - y + 1$ is a predefined integer chosen such that the Hankel matrix $\mathbf{H}^{\omega} = \mathcal{P}\_\{\mathcal{H}\}(\mathbf{D}^{\omega})$ is close to square. $\mathcal{P}\_\{\mathcal{R}\}$ is a rank-reducing operator to calculate a low-rank approximation of $\mathbf{H}^{\omega}$ by using the truncated SVD method (Golub and Loan, 1996; Shen et al., 2020):

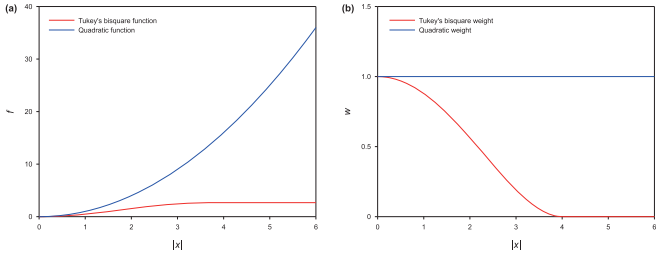

Fig. 1. Comparison of Tukey's bisquare and quadratic **(a)** norms, and **(b)** weights.

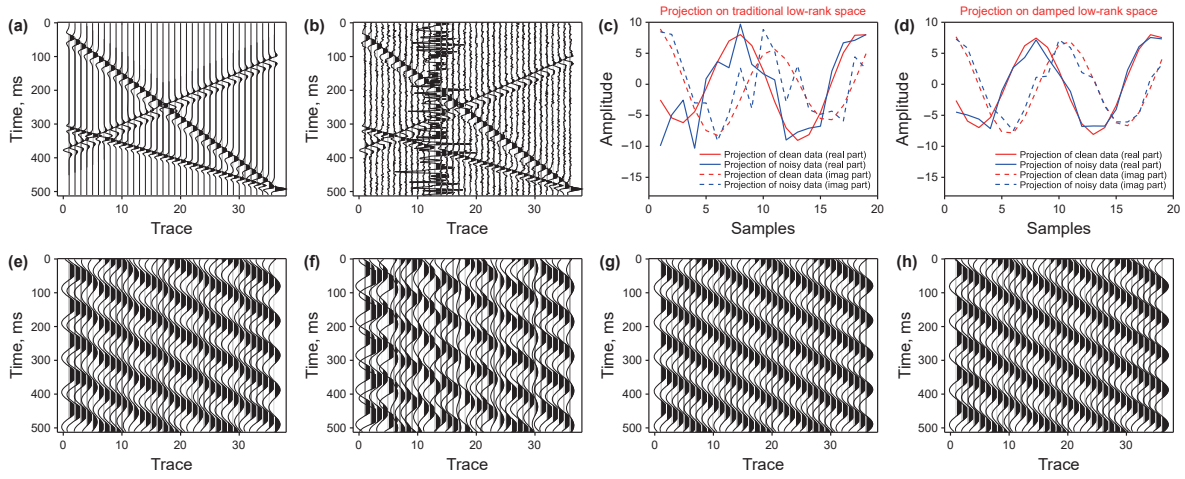

Fig. 2. Comparison of traditional and damped low-rank projections (demonstrated at 12 Hz harmonic frequency). **(a, b)** Clean and noisy data. **(c)** Projections of clean and noisy data on traditional low-rank space. **(d)** Projections of clean and noisy data on damped low-rank space. **(e, f)** Reconstructions of clean and noisy data with traditional low-rank projection. **(g, h)** Reconstructions of clean and noisy data with damped low-rank projection.

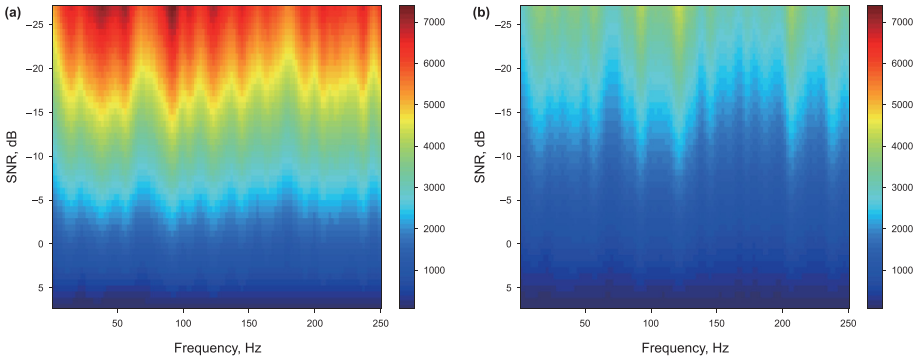

Fig. 3. Analysis of the traditional and damped low-rank projections. **(a)** Error map of the traditional low-rank projection. **(b)** Error map of the damped low-rank projection.

$$\overline{\mathbf{H}}^{\omega} = \mathcal{P}_{-}\{\mathcal{R}\}(\mathbf{H}^{\omega}) = \mathbf{U}_1^{\omega}\mathbf{\Sigma}_1^{\omega}(\mathbf{V}_1^{\omega})^{\mathrm{H}}, \tag{5}$$

where $\overline{\mathbf{H}}^{\omega}$ represents a low-rank approximation of $\mathbf{H}^{\omega}$. $\mathbf{\Sigma}_1^{\omega}$, $\mathbf{U}_1^{\omega}$ and $\mathbf{V}_1^{\omega}$ denote the first k largest singular values and associated k singular vectors of the matrix $\mathbf{H}^{\omega}$. $(\ )^{\mathrm{H}}$ denotes the Hermitian transpose of a matrix. The nature of the rank-reducing operator $\mathcal{P}_{-}\{\mathcal{R}\}$ is actually to solve the following inverse problem with an equality constraint:

$$\min \frac{1}{2}\|\mathbf{H}^{\omega} - \overline{\mathbf{H}}^{\omega}\|_{\mathrm{F}}^2, \quad s.t. \quad rank(\overline{\mathbf{H}}^{\omega}) = k, \tag{6}$$

where $\|\cdot\|_{\mathrm{F}}^2$ denotes Frobenius norm. k is an integer which is generally chosen as the number of the dipping components (e.g. $k = 3$ when the data have 3 different dipping events). $\mathcal{P}_{-}\{\mathcal{A}\}$ is an averaging operator which averages the anti-diagonals of the matrix $\overline{\mathbf{H}}^{\omega}$ to recover the filtered data $\mathbf{S}'^{\omega} = \mathcal{P}_{-}\{\mathcal{A}\}(\overline{\mathbf{H}}^{\omega})$. More details of the SSA approach are further explained in the work (Oropeza and Sacchi, 2011).

Although the SSA method is effective in suppression of seismic incoherent noise, it may perform unsteadily when the amplitudes of noise are dramatically larger than other samples. This is often the case when the field seismic data are corrupted with swell noise, power line noise, air blast noise, artifacts caused by glitches, recording errors and uncorrected polarity reversals. One of the most important reasons is that the SSA method seeks a low-rank approximation of the Hankel matrix of the observed data with a

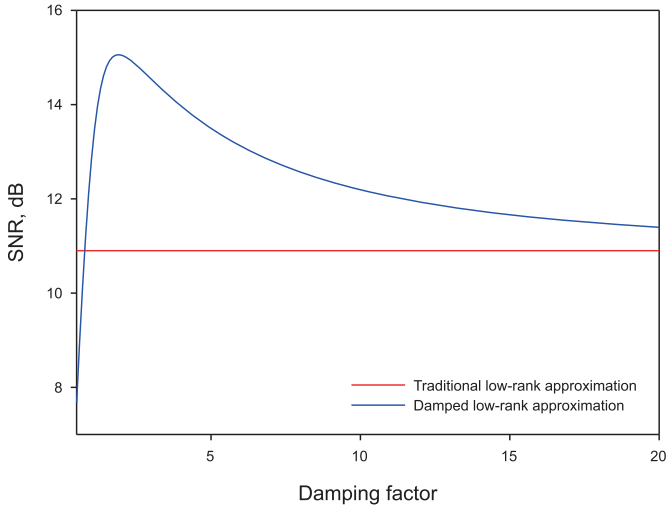

Fig. 4. SNR varies with different damping factors. The red line is the output SNR of the traditional low-rank approximation and the blue line is that of the damped low-rank approximation. The SNR curve of the damped low-rank approximation first increases and then decreases as the damping factor increases.

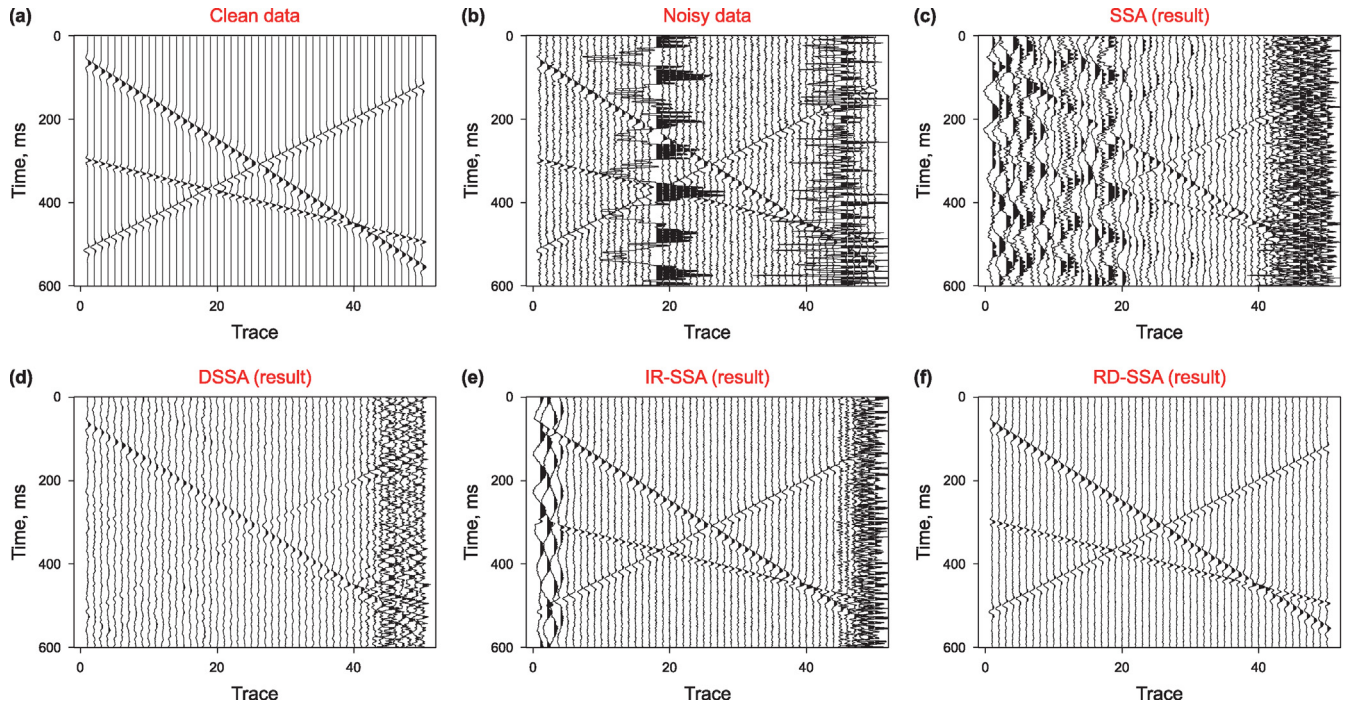

Fig. 5. Comparison of different low-rank reconstructions of linear events. **(a)** Clean data. **(b)** Noisy data corrupted by Gaussian and erratic noise. **(c)**–**(f)** low-rank reconstructions (denoising) by the SSA, DSSA, IR-SSA and RD-SSA methods, respectively.

quadratic misfit function. The quadratic misfit function will assign a large function value when the observed and calculated data have great differences in some samples, which makes the approximation quite sensitive to outliers.

2.2.1. Reweighting operation

One possible way to solve such problem is to replace the quadratic misfit function with a nonquadratic misfit function to robustify the low-rank approximation. For this end, the proposed reweighted damped SSA (RD-SSA) method adopts the Tukey's bisquare function (Beaton and Tukey, 1974) as

$$f_{\mathrm{T}}(x)=\begin{cases}\epsilon^2/6, & |x|>\epsilon;\\ \epsilon^2\left(1-\left(1-(x/\epsilon)^2\right)^3\right)/6, & |x|\le\epsilon,\end{cases} \tag{7}$$

where ε is a constant. Replacing the Frobenius norm with the Tukey's bisquare norm, the inverse problem in Eq. (6) is rewritten as

$$\min\frac{1}{2}f_{\mathrm{T}}(\mathbf{H}^{\omega}-\overline{\mathbf{H}}^{\omega}),\quad s.t.\ \ rank(\overline{\mathbf{H}}^{\omega})=k, \tag{8}$$

The minimization in Eq. (8) is a nonconvex optimization problem because the Tukey's bisquare norm is a nonquadratic norm. There is no closed-form solution for such inverse problem if a nonquadratic norm is chosen for the fidelity term (Chen and Sacchi, 2014). A reweighted least-squares strategy can be used to reach the minimization of a nonconvex optimization problem as

$$\min\frac{1}{2}\|\mathcal{P}_{-}\{\mathcal{H}\}(\mathbf{W})\odot(\mathbf{H}^{\omega}-\overline{\mathbf{H}}^{\omega})\|_F^2,\quad s.t.\ \ rank(\overline{\mathbf{H}}^{\omega})=k, \tag{9}$$

where $\odot$ is the Hadamard product. $\mathbf{W}=[w_{i,j}]$ is a reweighting matrix and its element $w_{i,j}$ is determined as

$$\mathbf{W}=[w_{i,j}]=\begin{cases}0, & |\gamma_{i,j}|>\epsilon;\\ (1-(\gamma_{i,j}/\epsilon)^2)^2, & |\gamma_{i,j}|\le\epsilon,\end{cases} \tag{10}$$

where $\gamma_{i,j}$ is the ith row and jth column element of the absolute difference $|\mathbf{D}^{\omega}-\mathbf{S}'^{\omega}|$. ε is related to the normalized median absolute deviation (MAD) and can be chosen as $4.685\cdot MAD$ (Holland and Welsch, 1977). Eq. (10) can be simply represented as $\mathbf{W}=g_{\mathrm{T}}(|\mathbf{D}^{\omega}-\mathbf{S}'^{\omega}|)$, where ε actually acts as a threshold to find out outliers, in other words, the (i, j) sample is considered as an outlier sample when $|\gamma_{i,j}|>\varepsilon$. Fig. 1(a) demonstrates a comparison of the Tukey's

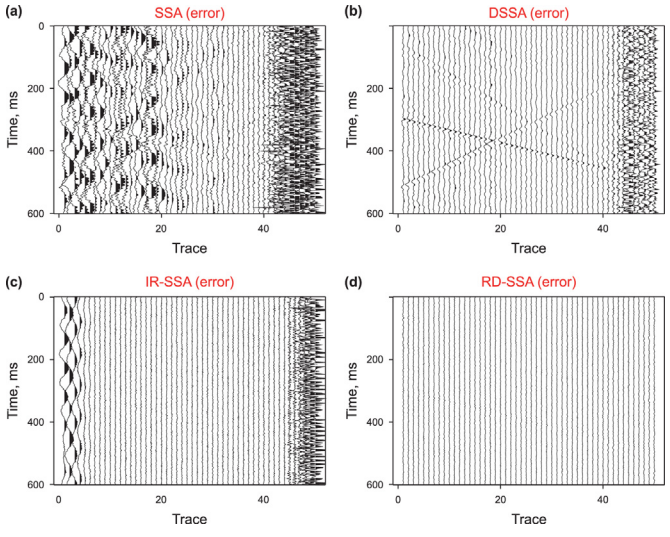

Fig. 6. Denoising errors of **(a)** SSA, **(b)** DSSA, **(c)** IR-SSA and **(d)** RD-SSA. Denoising errors refer to the differences between the clean data and the denoised data.

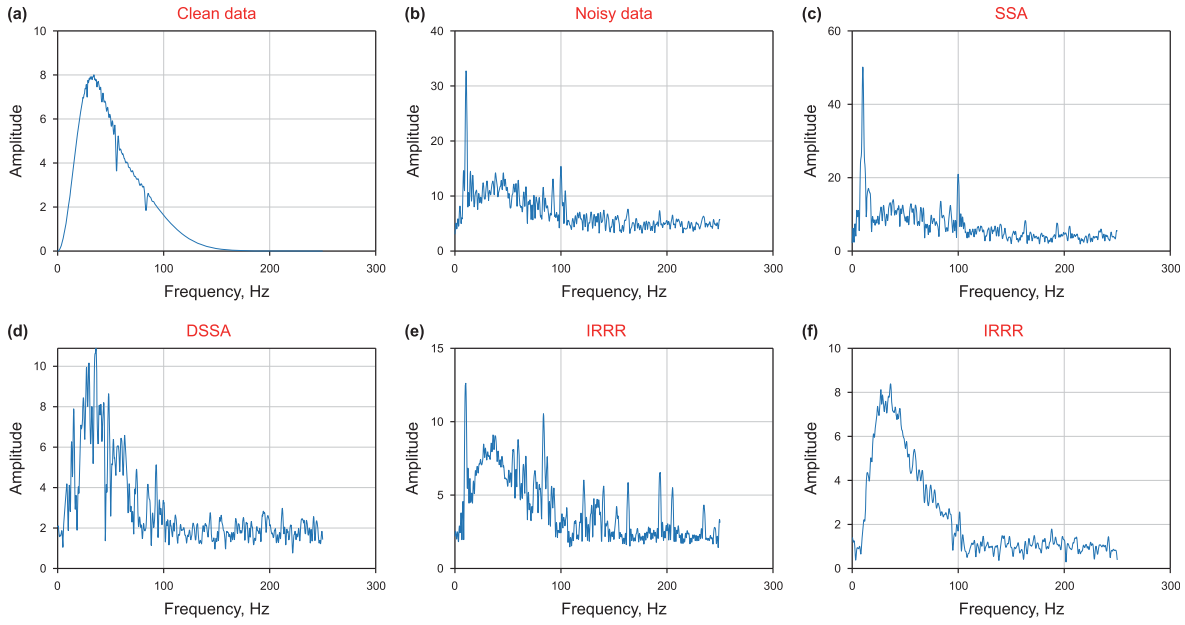

Fig. 7. The amplitude spectra of Fig. 5(a)–(f): **(a)** Clean data. **(b)** Noisy data corrupted by Gaussian and erratic noise. **(c)**–**(f)** low-rank reconstructions (denoising) by the SSA, DSSA, IR-SSA and RD-SSA methods, respectively.

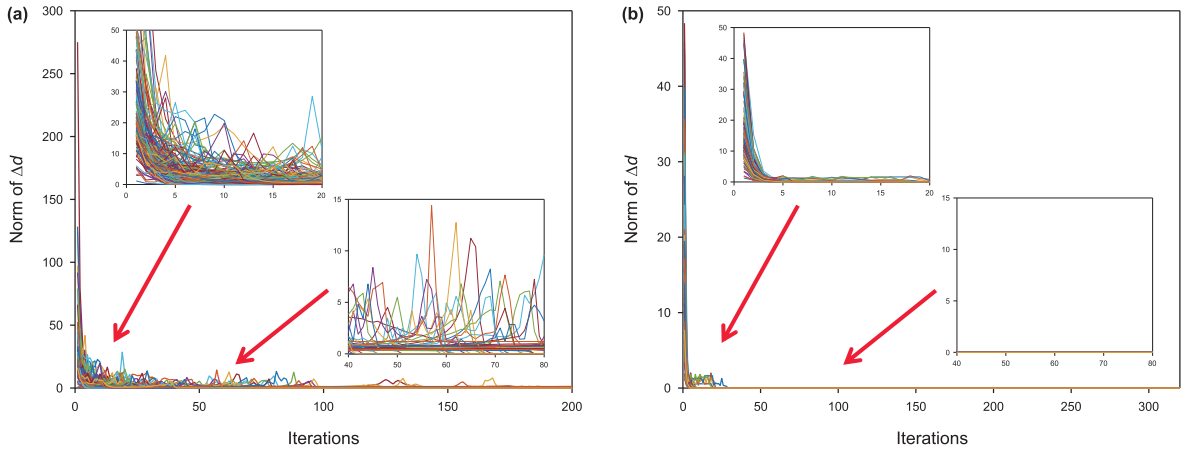

Fig. 8. Convergence curves of different harmonic frequencies (different colored lines) of **(a)** IR-SSA and **(b)** RD-SSA. In each figure, two detailed parts of convergence curves are magnified as highlighted by the red arrows. The vertical coordinate represents the L2 norm of the difference between two consecutive results in the iteration process.

bisquare and quadratic norm, and Fig. 1(b) demonstrates the corresponding weights. It can be observed that the outlier sample will be assigned a small weight with the Tukey's bisquare norm, which can make the inversion process less sensitive to outlier samples.

2.2.2. Damping operation

It can be observed that the reweighting matrix $\mathbf{W}$ is closely related to the low-rank approximation $\overline{\mathbf{H}}^{\omega}$. Although we have an analytic expression for solving Eq. (9) given by the truncated SVD, as used in the traditional SSA filtering, it may fail for the strong erratic disturbance because the truncated SVD is the least-squares solution of the low-rank problem. From the knowledge of linear algebra, the SVD of matrix $\mathbf{H}^{\omega}$ can be represented as

$$\mathbf{H}^{\omega} = \begin{pmatrix} \mathbf{U}_1^{\omega} & \mathbf{U}_2^{\omega} \end{pmatrix} \begin{pmatrix} \mathbf{\Sigma}_1^{\omega} & 0 \\ 0 & \mathbf{\Sigma}_2^{\omega} \end{pmatrix} \begin{pmatrix} (\mathbf{V}_1^{\omega})^{\mathrm{H}} \\ (\mathbf{V}_2^{\omega})^{\mathrm{H}} \end{pmatrix}, \tag{11}$$

where the subscript 1 and 2 denote the first k largest and the rest singular values and associated singular vectors, respectively. The truncated SVD for rank-k approximation is achieved by abandoning $\mathbf{\Sigma}_2^{\omega}$ and its associated singular vectors, which decomposes the data into a noise subspace and a signal-plus-noise subspace. Due to the strong amplitudes of the erratic disturbances, the projection on the low-rank space is easy to produce serious distortion. To address this problem, we introduce a damping operator into the low-rank approximation as (Huang et al., 2016)

$$\tilde{\mathbf{H}}^{\omega} = \overline{\mathcal{P}_R}(\mathbf{H}^{\omega}) = \mathbf{U}_1^{\omega}\mathbf{\Sigma}_1^{\omega}\mathbf{T}(\mathbf{V}_1^{\omega})^{\mathrm{H}}, \tag{12}$$

$$\mathbf{T} = \mathbf{I} - (\mathbf{\Sigma}_1^{\omega})^{-N}\delta^{N} \tag{13}$$

where $\mathbf{T}$ is the damping operator, N is the damping factor, $\mathbf{I}$ is an identity matrix and δ is the maximum element of $\mathbf{\Sigma}_2^{\omega}$. Compared with the truncated SVD, this the damping operator changes the row space of the original low-rank approximation to attenuate the residual projection of noise. More mathematical foundations can be

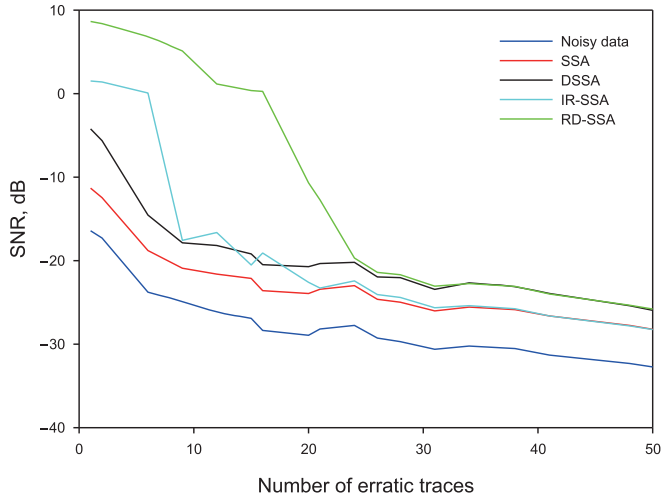

Fig. 9. Output SNR curves of different methods vary with different number of erratic traces.

found in Huang et al. (2016). It can also weaken the artificial disturbance introduced by the low-rank projection of erratic disturbances. The damping factor can be adjusted to project both erratic and random noise to an acceptable level and avoid the error accumulated with iterations.

Fig. 2 is a comparison of traditional and damped low-rank projections (demonstrated at 12 Hz harmonic frequency). In this comparison, we project a clean dataset (Fig. 2(a)) and a noisy dataset (Fig. 2(b)) on the traditional and damped low-rank spaces, respectively. The projection results on traditional and damped low-rank spaces are shown in Fig. 2(c) and (d), respectively. The red and blue lines denote the projections of the clean and noisy data, respectively. The solid and dashed lines denote the real and imaginary parts, respectively. Fig. 2(e) and (f) are the denoising results of clean and noisy data with traditional low-rank projection, and Fig. 2(g) and (h) are those with the damped low-rank projection. It is clear that the erratic noise changes the projected curves on the traditional low-rank space significantly (Fig. 2(c)). The damped low-rank projection shows decent robustness to the erratic noise (Fig. 2(d)), in which the reconstruction result of the clean data (Fig. 2(g)) has almost no change after erratic noise corruption (Fig. 2(h)). Fig. 3 presents the error analysis of the traditional and damped low-rank projections varying with different harmonic frequencies and levels of additive erratic noise. The error refers to the root-mean-square of the difference between the low-rank projections of the clean and noisy data. Fig. 3(a) corresponds to the traditional low-rank projection, and Fig. 3(b) corresponds to the damped low-rank projection. Within the error analysis, we can also see the superior robustness of the damped low-rank projection which can always hold smaller errors. Fig. 4 presents a reconstruction error curve varying with different damping factors. It can be seen that the error of the damped low-rank reconstruction decreases as the damping factor decreases, when the damping factor is not very small. However, users need to be careful to choose a small damping factor because it may produce a huge reconstruction error.

2.2.3. Algorithm implementation

The DR-SSA method is implemented by alternately solving the reweighting matrix $\mathbf{W}$ and the low-rank filtered data $\mathbf{S}'^{(\omega)}$, which can be represented mathematically as

$$\mathbf{S}_i'^{(\omega)} = \mathcal{P}_{-}\{\mathcal{A}\}(\overline{\mathcal{P}_R}(\mathcal{P}_{-}\{\mathcal{H}\}(\mathbf{D}_i^{(\omega)}))), \tag{14}$$

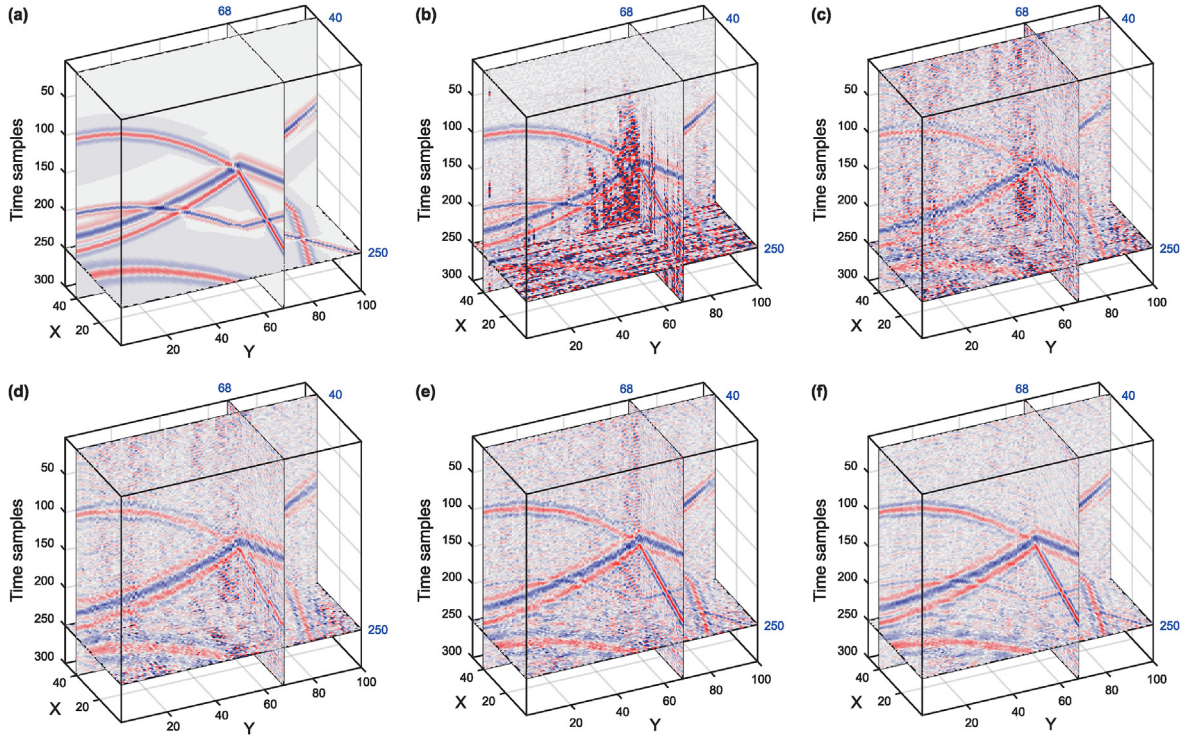

Fig. 10. Comparison of different low-rank reconstructions of curve events. **(a)** Clean data. **(b)** Noisy data corrupted by swell noise. **(c)**–**(f)** low-rank reconstructions (denoising) by the SSA, DSSA, IR-SSA and RD-SSA methods, respectively. In this experiment, all the four methods are implemented in local windows.

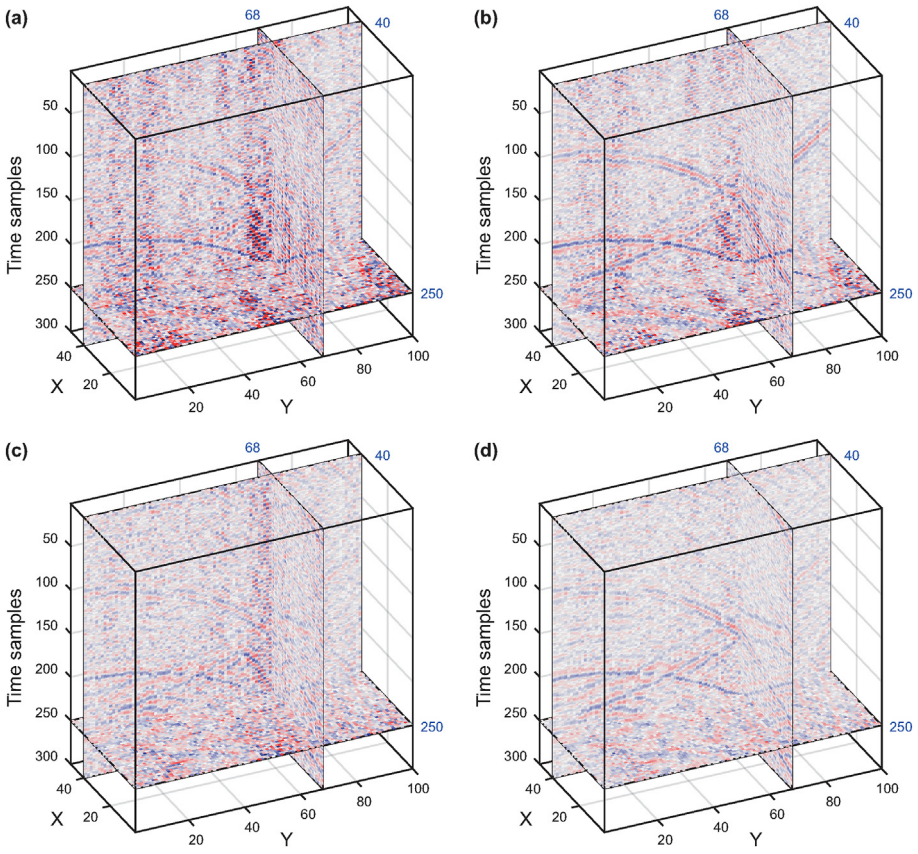

Fig. 11. Denoising errors of **(a)** SSA, **(b)** DSSA, **(c)** IR-SSA and **(d)** RD-SSA. Denoising errors refer to the differences between the clean data and the denoised data.

Table 1
SNRs (dB) of the results of the two synthetic examples.

	Input	SSA	DSSA	IR-SSA	RD-SSA
Linear events	−17.8896	−12.9447	−3.8732	−8.5054	8.2206
Curve events	−16.6395	−7.3268	−2.9926	−1.6592	1.9966

$$\mathbf{W}_i = g_{\mathrm{T}}\left(\left|\mathbf{D}^{\omega} - \mathbf{S}_i^{\prime\omega}\right|\right), \tag{15}$$

$$\mathbf{D}_{i+1}^{\omega} = \mathbf{D}^{\omega} \odot \mathbf{W}_i + \mathbf{S}_i^{\prime\omega} \odot (\mathbf{I} - \mathbf{W}_i), \tag{16}$$

where I is a matrix with all elements equalling 1, i is the iteration index. Eqs. (14)–(16) are solved alternately to obtain the final solution. The central idea of RD-SSA is to iteratively approximate the observed data with the quadratic norm for the first iteration to obtain the initial $\mathbf{S}_1^{\prime\omega}$, and the Tukey's bisquare norm for the rest iterations. Similar to the traditional SSA method, the truncation rank k in the RD-SSA method is determined equalling to the number of the dipping components. The damping factor N increases with iteration as

$$N = N_{\mathrm{L}} + (N_{\mathrm{U}} - N_{\mathrm{L}}) \cdot i / I, \tag{17}$$

where N_{L} and N_{U} are the user-given lower and upper limits of the damping factor, respectively. I is the maximum iteration number. User has the flexibility to choose the criterion for maximum iteration number such as the absolute variation ratio, relative variation ratio or a specific number. A complete and detailed algorithm workflow of the proposed RD-SSA approach is given in Algorithm 1.

Algorithm 1. RD-SSA

Algorithm 1 RD-SSA

procedure INPUT($\mathbf{D}$, k, N_{L}, N_{U}, I, ω_{L}, ω_{U})
  $\mathbf{D}^{\omega} \leftarrow \mathbf{D}$ using Fourier transform
  for $\omega \leftarrow \omega_{\mathrm{L}} : \omega_{\mathrm{U}}$ **do**
    for $i \leftarrow 0 : I$ **do**
      $N \leftarrow N_{\mathrm{L}}, N_{\mathrm{U}}, i, I$ using equation Eq. 17
      $\mathbf{S}^{\prime\omega} \leftarrow \mathbf{D}^{\omega}, k, N$ using Eq. 14
      $\mathbf{W} \leftarrow \mathbf{S}^{\prime\omega}, \mathbf{D}^{\omega}$ using Eq. 15
      $\mathbf{D}^{\omega} \leftarrow \mathbf{W}, \mathbf{S}^{\prime\omega}, \mathbf{D}^{\omega}$ using Eq. 16
    end for
  end for
  $\mathbf{D} \leftarrow \mathbf{D}^{\omega}$ using inverse Fourier transform
end procedure

3. Example

3.1. Synthetic example

To simplify the numerical environment and highlight the performance comparison among different SSA-based methods, we use a synthetic dataset consisting of three linear events with different dips, polarities, and dominant frequencies. In this case, the rank for the SSA-based methods equals 3. It avoids different performances due to inapposite parameter selection. The clean data are shown in Fig. 5(a). Two noisy traces with high amplitudes and Gaussian noise is added to the clean data as shown in Fig. 5(b). The first example explores the performance of low-rank approximation of the linear events, which straightforwardly demonstrates the resistance to erratic disturbance. Fig. 5(c) and (d) are the denoised results by using the SSA (Trickett, 2008; Oropeza and Sacchi, 2011) and DSSA

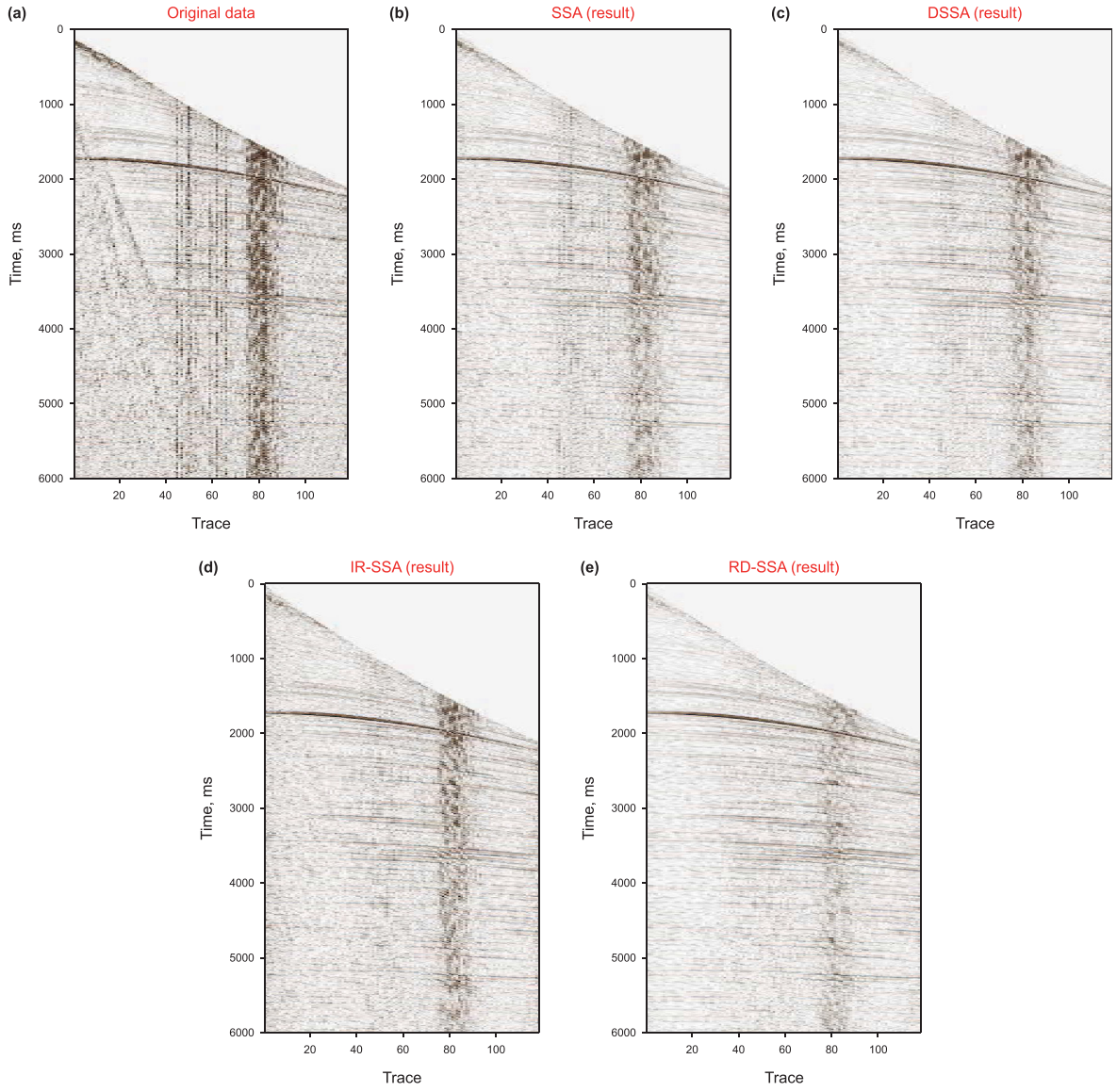

Fig. 12. The field data example. **(a)** Initial data. **(b)**–**(e)** Denoised results after using the SSA, DSSA, IR-SSA, and RD-SSA methods, respectively.

(Huang et al., 2016) methods, respectively. Fig. 5(e) and (f) are the results after using two iterative methods, namely the iterative robust SSA (IR-SSA) method (Trickett et al., 2012) and the proposed RD-SSA method, respectively. Fig. 6 shows the corresponding denoising errors given by the differences between clean data (Fig. 5(a)) and denoised results (Fig. 5(c)–(f)). The rank for all the four methods is 3. The damping factor for the DSSA method is 8, and linearly increases from 3 to 8 for the proposed RD-SSA method. The maximum iteration number for each frequency component of both the IR-SSA and RD-SSA methods is 200. The computation times for the four methods are 0.0871, 0.875, 5.3065 and 0.8775 respectively. The result demonstrates that the low-rank approximation with SSA (Fig. 5(c)) turns into an unstable state and generates a lot of factitious noise. Although the DSSA method (Fig. 5(d)) is more robust than the SSA method, it still introduces some noise in the last several traces. The IR-SSA method suppresses the erratic noise and estimates the clean data by iteratively implementing the SSA filtering, which can improve the robustness of the low-rank approximation. However, for the strong erratic noise, it also leaves significant artifacts as demonstrated in Fig. 5(e). On the contrary, the proposed RD-SSA method (Fig. 5(f)) successfully attenuates the erratic noise and shows a good resistance to erratic disturbances. Fig. 7 shows the amplitude spectra of the clean data (Fig. 5(a)), noisy data (Fig. 5(b)) and the four denoised results (Fig. 5(c)–(f)). It could be seen that the RD-SSA method keeps the dominant frequency, frequency band, and shape of the amplitude spectra better than other methods. Fig. 8 presents the convergence curves of different harmonic frequencies (different colored lines) of the IR-SSA and RD-SSA methods. In each figure, two detailed parts of convergence curves are magnified as highlighted by the red arrows. The RD-SSA method holds faster convergence than the IR-SSA method, which achieves convergence for all the frequency components with no more than 30 iterations. To make the comparsion more comprehensive, Fig. 9 demonstrates SNRs of the denoised results using different methods vary with different number of erratic traces. The SNR is calculated as (Huang and Wang, 2018)

$$SNR = 10\log\frac{\|CLEAN\|_F^2}{\|CLEAN - NOISY\|_F^2}, \tag{18}$$

where *CLEAN* represents the clean data, and *NOISY* represents the

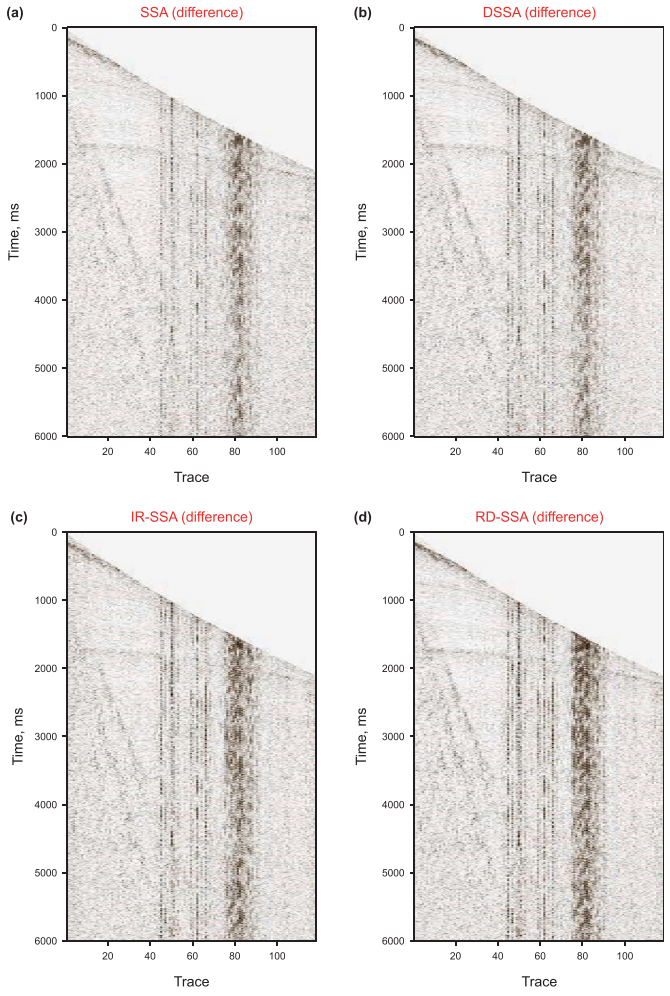

Fig. 13. The difference sections between the original data (Fig. 12(a)) and denoised results **(a)** SSA, **(b)** DSSA, **(c)** IR-SSA, and **(d)** RD-SSA.

noisy data.

The second synthetic example explores the performance of low-rank approximation of the 3D curve events. Because the SSA-based method relies on the assumption of plane waves, all the four methods are implemented in local spatial windows (20×20 traces) to make the data close to the ideal signal model meeting the low-rank assumption. 50% overlapping is allowed for every two adjacent windows to eliminate the windowing effect. Fig. 10(a) and (b) are the clean data and the noisy data corrupted by swell noise. The swell noise in Fig. 10(b) is extracted from a field dataset. The denoised results using the SSA, DSSA, IR-SSA, RD-SSA approaches are shown in Fig. 10(c)–(f), respectively. The denoising errors are presented in Fig. 11. For this experiment, the ranks for all the four methods are 4. The damping factor for the DSSA method is 8, and linearly increases from 3 to 6 for the proposed RD-SSA method. The maximum iteration number for each frequency component of both the IR-SSA and RD-SSA methods is 20. All the parameters are kept the same for each local window. The computation times for the four methods are 59.094, 61.224, 322.021 and 104.975 respectively. As observed from the results, the SSA reconstruction section is very noisy with strong energies of erratic noise developed. It is because the sensibility of erratic disturbance of SSA, which introduces artifacts. The denoising results of both the DSSA and IR-SSA methods are much more robust than that of SSA, which attenuate most energies of the two traces with erratic noise but still introduce artifacts. Comparing the denoising results and errors, the proposed RD-SSA method performs better than other methods. Table 1 shows the quantitative analysis of signal to noise ratio (SNR) of the two synthetic examples.

3.2. Field example

A field data example is used to further demonstrate the effectiveness of the proposed RD-SSA method. The original field dataset is a CMP dataset and has 120 traces and 1500 time-samples per trace as shown in Fig. 12(a). The original data are contaminated by some erratic energies within the area around trace 40–90. In addition, the original data are contaminated by incoherent ambient

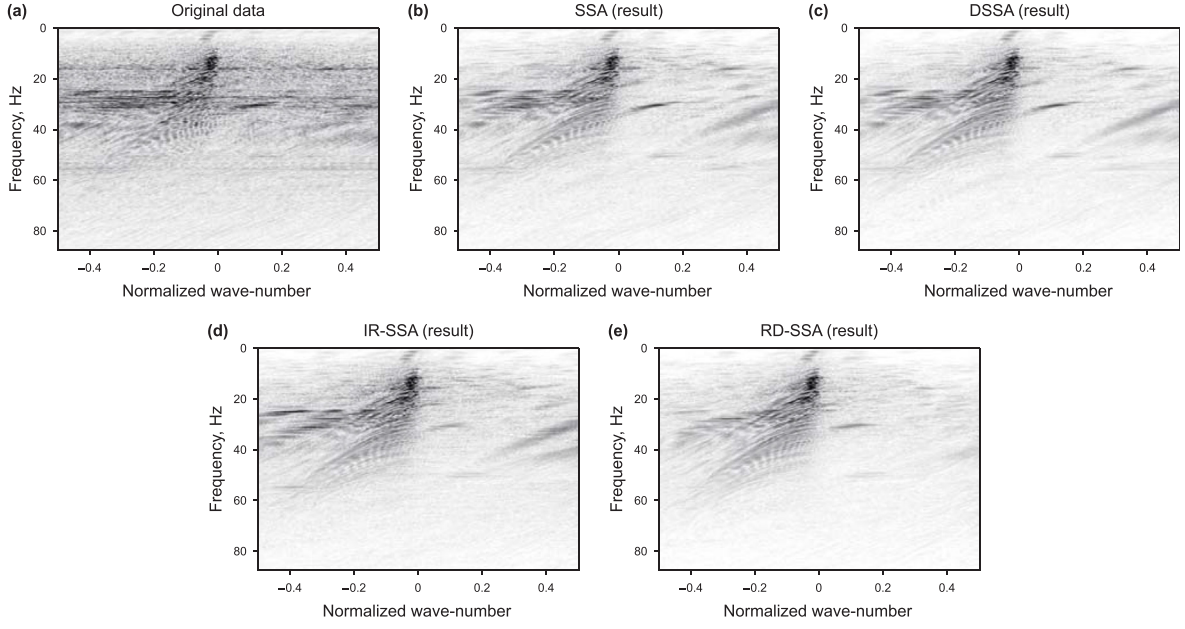

Fig. 14. The $f - k$ spectra of Fig. 12**(a)**–**(e)**, respectively.

noise and some residual ground roll. Most of the ground roll energy is removed in advance and the residual presents poor coherency. Thus, these poorly coherent energies can be roughly treated as incoherent noise and eliminated by incoherent noise attenuation techniques. Similar to the synthetic example, the SSA, DSSA, IR-SSA and RD-SSA algorithms are applied to suppress the incoherent noise. Theoretically, the rank equals the number of dipping events. For the field seismic data, it is hard to determine such number. Therefore, rank for the field seismic data is generally the determined by the try-and-error method. All the four methods are implemented in local windows of 40 traces. The rank is 6 for all the four methods. The damping factor for the DSSA method is 6, and linearly increases from 3 to 6 for the proposed RD-SSA method. The maximum iteration number for each frequency component of both the IR-SSA and RD-SSA methods is 200. The computation times for the four methods are 2.051, 2.325, 80.632 and 45.604 respectively. The denoised results are shown in Fig. 12(b)–(e). The four difference sections (i.e., the difference between the original data (Fig. 12(a)) and the four denoised results (Fig. 12(b)–(e)) are presented in Fig. 13. It can be confirmed that all the four SSA-based methods suppress the incoherent noise to some extent. However, the RD-SSA method performs better and obtains a cleaner seismic profile. From all the SSA, DSSA, and IR-SSA denoised results (Fig. 12(b)–(d)) we can still observe residual erratic noise. There are no notable signal leakages in all the four difference sections (Fig. 13) which suggests that the signals are preserved well after using all the four denoising methods. Fig. 14(a)–(e) show the $f-k$ spectra of Fig. 12(b)–(e), respectively. For a close observation, the small data sections of trace 65–75 and 2400–3200 ms are magnified from the original data and the four denoised data, as shown in Fig. 15. The results show that, the events' consistencies are much improved after using the proposed RD-SSA method as highlighted by the blue lines, which indicates a successful performance.

4. Discussion

There are two main shortcomings of the proposed RD-SSA method. The one is the computational efficiency. On the one hand, the RD-SSA method needs to take many iterations to obtain the final result, and will inevitably have more computational time than the non-iterative method, for instance, the traditional SSA method. Therefore, to attenuate the incoherent noise without high

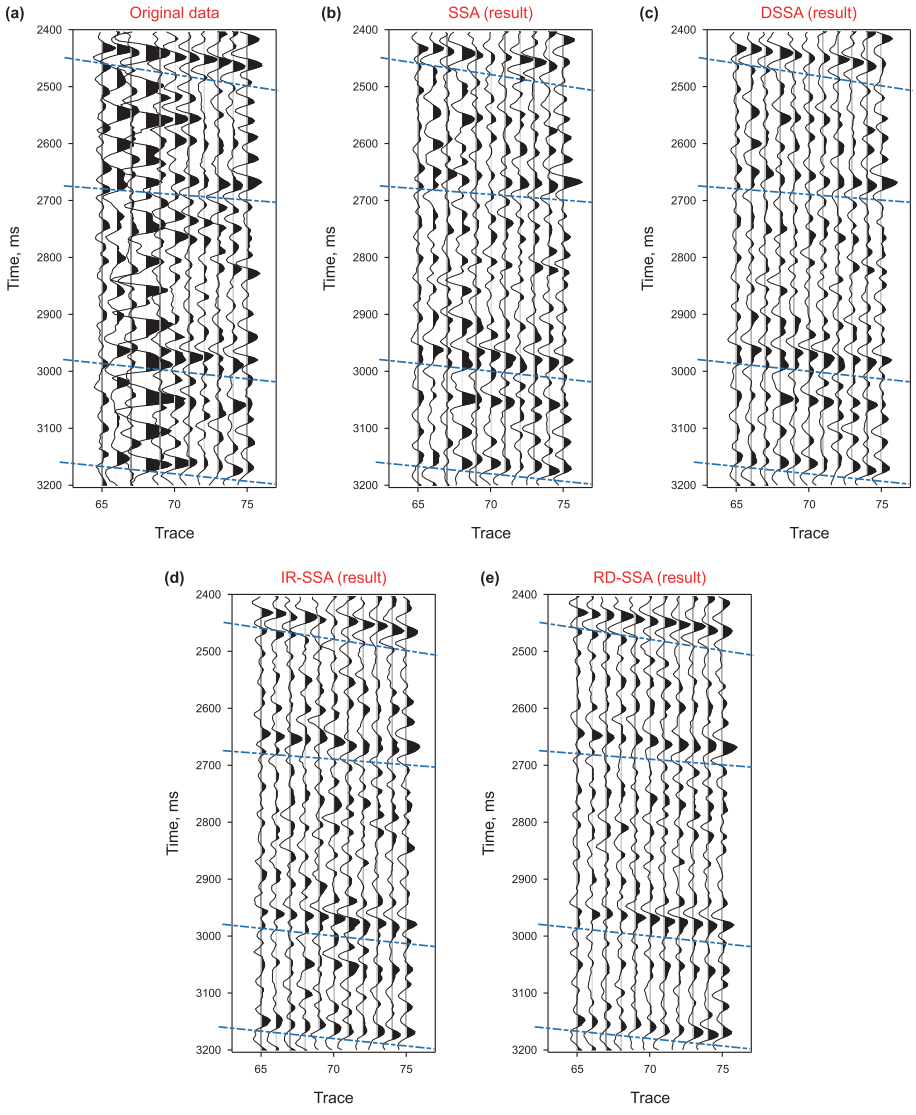

Fig. 15. The magnified sections of **(a)** initial data, and **(b)**–**(e)** denoised results after using the SSA, DSSA, IR-SSA, and RD-SSA methods, respectively.

amplitudes, the traditional SSA method is recommended because it is more efficient. On the other hand, the RD-SSA method needs the SVD of the explicit matrix (which is stored in memory). 5D applications of the SSA would build matrices that are too big for this case, and the SVD is prohibitive in this case. The other is that the RD-SSA method has a limited performance in suppression of coherent noise, such as multiples and linear interference. The main reason is that the coherent noise, especially those with high apparent velocities, have well consistencies in adjacent traces and therefore accord with low-rank assumption of the Hankel matrix (Huang et al., 2017b). The coherent noise is hard to separate from the signal by the SSA-based method because they are mixed in the singular spectrum. One possible solution is to introduce a randomization operator following Huang et al. (2017b), to destroy the consistency of the coherent noise prior to the SSA filtering.

Compared with the existing robust SSA variants, there are two main contributions. The first one is that it finds the damping operator can not only improve the performance of SSA to separate signal and noise, but also improve its robustness to erratic noise. Another is that it incorporates the damping operator into a Tukeys bisquare norm-based iteratively reweighting framework, in which the damping operator changes with iterations. In the early phase of iterations, it imposes a strong damping effect to attenuate the artificial disturbance introduced by the low-rank projection of the erratic noise. In the late phase of iterations, it imposes a weak damping effect to accelerate convergence and preserve the signal amplitude.

5. Conclusions

We have further extended the DSSA method to robustify the low-rank reconstruction of seismic data, and proposed a reweighted version of DSSA (RD-SSA) for robust seismic noise suppression. With the damping operator interposing, the RD-SSA method can weaken the artificial disturbance introduced by the low-rank projection of both erratic and random noise. The damping factor can be adjusted to project both erratic and random noise to an acceptable level and avoid the error accumulated with iterations. The Tukey's bisquare measure is adopted to make the inversion process of denoising less sensitive to the outlier samples. The RD-SSA updates alternately Tukey's bisquare weight and the low-rank approximation within iterations. Based on the application on both synthetic and field data examples, despite the higher computational costs due to its iterative nature, the RD-SSA method offers a good performance in the seismic incoherent noise suppression and exhibits robustness to strong erratic disturbances compared with the SSA, DSSA and IR-SSA methods.

CRediT authorship contribution statement

Wei-Lin Huang: Writing – review & editing, Writing – original draft, Software, Methodology. **Yan-Xin Zhou:** Writing – review & editing, Visualization. **Yang Zhou:** Writing – review & editing, Methodology. **Wei-Jie Liu:** Writing – review & editing, Writing – original draft, Methodology, Investigation. **Ji-Dong Li:** Writing – review & editing, Writing – original draft.

Declaration of competing interest

The authors declare that they have no known competing financial interests or personal relationships that could have appeared to influence the work reported in this paper.

Acknowledgments

This work was supported by the National Natural Science Foundation of China under grant no. 42374133, and the Beijing Nova Program under grant no. 2022056, and the Fundamental Research Funds for the Central Universities under grant no. 2462020YXZZ006, and the Young Elite Scientists Sponsorship Program by CAST (YESS) under grant no. 2018QNRC001. We would like to thank four anonymous reviewers for their constructive suggestions.

References

Anvari, R., Mohammadi, M., Kahoo, A.R., 2019. Enhancing 3-D seismic data using the t-SVD and optimal shrinkage of singular value. IEEE J. Sel. Top. Appl. Earth Obs. Rem. Sens. 12, 382–388. https://doi.org/10.1109/JSTARS.2018.2883404.

Anvari, R., Siahsar, M.A.N., Gholtashi, S., Kahoo, A.R., Mohammadi, M., 2017. Seismic random noise attenuation using synchrosqueezed wavelet transform and low-rank signal matrix approximation. IEEE Trans. Geosci. Rem. Sens. 55, 6574–6581. https://doi.org/10.1109/TGRS.2017.2730228.

Bahia, B., Sacchi, M., 2019. Robust singular spectrum analysis via the bifactored gradient descent algorithm. In: SEG Technical Program Expanded Abstracts 2019. Society of Exploration Geophysicists, pp. 4640–4644. https://doi.org/10.1190/segam2019-3215465.1.

Beaton, A.E., Tukey, J.W., 1974. The fitting of power series, meaning polynomials, illustrated on band-spectroscopic data. Technometrics 16, 147–185. https://doi.org/10.1080/00401706.1974.10489171.

Bekara, M., van der Baan, M., 2009. Random and coherent noise attenuation by empirical mode decomposition. Geophysics 74, V89–V98. https://doi.org/10.1190/1.3063881.

Chen, K., Sacchi, M.D., 2014. Robust reduced-rank filtering for erratic seismic noise attenuation. Geophysics 80, V1–V11. https://doi.org/10.1190/geo2014-0116.1.

Chen, X., Cao, J.-J., Yang, H.-L., Shi, S.-J., Guo, Y.-S., 2022. Diffraction separation and imaging based on double sparse transforms. Petrol. Sci. 19, 534–542. https://doi.org/10.1016/j.petsci.2021.12.002.

Chen, Y., Zhang, M., Bai, M., Chen, W., 2019. Improving the signal-to-noise ratio of seismological datasets by unsupervised machine learning. Seismol Res. Lett. 90, 1552–1564. https://doi.org/10.1785/0220190028.

Cheng, J., Chen, K., Sacchi, M.D., 2015. Application of robust principal component analysis (RPCA) to suppress erratic noise in seismic records. In: SEG Technical Program Expanded Abstracts 2015. Society of Exploration Geophysicists, pp. 4646–4651. https://doi.org/10.1190/segam2015-5869427.1.

Cheng, J., Sacchi, M.D.. A fast rank-reduction algorithm for 3D deblending via randomized QR decomposition, pp. 3830–3835. https://doi.org/10.1190/segam2015-5850767.1.

Ding, Y., Selesnick, I.W., 2015. Artifact-free wavelet denoising: non-convex sparse regularization, convex optimization. IEEE Signal Process. Lett. 22, 1364–1368. https://doi.org/10.1109/LSP.2015.2406314.

Golub, G.H., Loan, C.F.V., 1996. Matrix Computations. The Johns Hopkins University Press.

Gómez, J.L., Velis, D.R., 2016. A simple method inspired by empirical mode decomposition for denoising seismic data. Geophysics 81, V403–V413. https://doi.org/10.1190/geo2015-0566.1.

Herrmann, F.J., Hennenfent, G., 2008. Non-parametric seismic data recovery with curvelet frames. Geophys. J. Int. 173, 233–248. https://doi.org/10.1111/j.1365-246X.2007.03698.x.

Holland, P.W., Welsch, R.E., 1977. Robust regression using iteratively reweighted least-squares. Commun. Stat. 6, 813–827. https://doi.org/10.1080/03610927708827533.

Huang, W., Liu, J., 2020. Robust seismic image interpolation with mathematical morphological constraint. IEEE Trans. Image Process. 29, 819–829. https://doi.org/10.1109/TIP.2019.2936744.

Huang, W., Wang, R., 2018. Random noise attenuation by planar mathematical morphological filtering. Geophysics 83, V11–V25. https://doi.org/10.1190/geo2017-0288.1.

Huang, W., Wang, R., Chen, Y., Li, H., Gan, S., 2016. Damped multichannel singular spectrum analysis for 3D random noise attenuation. Geophysics 81, V261–V270. https://doi.org/10.1190/geo2015-0264.1.

Huang, W., Wang, R., Li, H., Chen, Y., 2017a. Unveiling the signals from extremely noisy microseismic data for high-resolution hydraulic fracturing monitoring. Sci. Rep. 7, 11996.

Huang, W., Wang, R., Yuan, Y., Gan, S., Chen, Y., 2017b. Signal extraction using randomized-order multichannel singular spectrum analysis. Geophysics 82, V69–V84.

Lan, N.-Y., Zhang, F.-C., Yin, X.-Y., 2022. Seismic data reconstruction based on low dimensional manifold model. Petrol. Sci. 19, 518–533. https://doi.org/10.1016/j.petsci.2021.10.014.

Li, H., Wang, R., Cao, S., Chen, Y., Huang, W., 2016. A method for low-frequency noise suppression based on mathematical morphology in microseismic monitoring. Geophysics 81, V159–V167. https://doi.org/10.1190/geo2015-0222.1.

Li, L., Zhang, G.-Z., Liu, J.-Z., Han, L., Zhang, J.-J., 2021. Estimation of fracture density

and orientation from azimuthal elastic impedance difference through singular value decomposition. Petrol. Sci. 18, 1675–1688. https://doi.org/10.1016/j.petsci.2021.09.037.
Li, Z.-C., Qu, Y.-M., 2022. Research progress on seismic imaging technology. Petrol. Sci. 19, 128–146. https://doi.org/10.1016/j.petsci.2022.01.015.
Lin, R., Bahia, B., Sacchi, M.D., 2021. Iterative deblending of simultaneous-source seismic data via a robust singular spectrum analysis filter. IEEE Trans. Geosci. Rem. Sens. 60, 1–10. https://doi.org/10.1109/TGRS.2021.3086834.
Mousavi, S.M., Langston, C.A., Horton, S.P., 2016. Automatic microseismic denoising and onset detection using the synchrosqueezed continuous wavelet transform. Geophysics 81 (4), V341–V355. https://doi.org/10.1190/geo2015-0598.1.
Naghizadeh, M., Sacchi, M., 2013. Multidimensional de-aliased Cadzow reconstruction of seismic records. Geophysics 78, A1–A5. https://doi.org/10.1190/segam2012-0494.1.
Oropeza, V., Sacchi, M., 2011. Simultaneous seismic data denoising and reconstruction via multichannel singular spectrum analysis. Geophysics 76, V25–V32. https://doi.org/10.1190/1.3552706.
Sacchi, M.D. Fx Singular Spectrum Analysis. Cspg Cseg Cwls Convention, Citeseer, 392–395. https://www.researchgate.net/publication/255663970.
Shen, H.Y., Li, Q., Yan, Y.Y., Li, X.X., Science, P., 2020. Separation of diffracted waves via svd filter. Petrol. Sci. 1–13. https://doi.org/10.1007/s12182-020-00480-8.
Sternfels, R., Viguier, G., Gondoin, R., Le Meur, D., 2015. Multidimensional simultaneous random plus erratic noise attenuation and interpolation for seismic data by joint low-rank and sparse inversion. Geophysics 80, WD129–WD141. https://doi.org/10.1190/geo2015-0066.1.
Trad, D.O., Ulrych, T.J., Sacchi, M.D., 2002. Accurate interpolation with high-resolution time-variant radon transforms. Geophysics 67, 644–656. https://doi.org/10.1190/1.1468626.
Trickett, S., 2008. F-xy cadzow noise suppression. In: SEG Technical Program Expanded Abstracts 2008. Society of Exploration Geophysicists, pp. 2586–2590. https://doi.org/10.1190/1.3063880.
Trickett, S., Burroughs, L., Milton, A., 2012. Robust rank-reduction filtering for erratic noise: SEG technical program expanded abstracts 2008. Society of Exploration Geophysicists SEG–2012. https://doi.org/10.1190/segam2012-0129.1.
Wang, R., Li, Q., Zhang, M., 2008. Application of multi-scaled morphology in denoising seismic data. Appl. Geophys. 5, 197–203. https://doi.org/10.1007/s11770-008-0033-3.
Wang, Y.-Q., Wang, Q., Lu, W.-K., Ge, Q., Yan, X.-F., 2022. Seismic impedance inversion based on cycle-consistent generative adversarial network. Petrol. Sci. 19, 147–161. https://doi.org/10.1190/segam2019-3203757.1.
Wu, B., Yu, J., Ren, H., Lou, Y., Liu, N., 2020. Seismic traffic noise attenuation using lp-norm robust PCA. Geosci. Rem. Sens. Lett. IEEE 17, 1998–2001. https://doi.org/10.1109/LGRS.2019.2955737.
Zhu, Z., Cao, D., Wu, B., 2019. Seismic high amplitude noise attenuation based on the deep learning method: 81st EAGE conference and exhibition 2019. Eur. Assoc. Geoscientists Eng. 1–5. https://doi.org/10.3997/2214-4609.201901356.
Zwartjes, P., Gisolf, A., 2007. Fourier reconstruction with sparse inversion. Geophys. Prospect. 55, 199–221. https://doi.org/10.1111/j.1365-2478.2006.00580.x.